Journal of
Biomedical Nanotechnology
Vol. 1, 1–7, 2005

Arrays of Microfluidically-Addressable Nanoholes

T. Fettah Kosar, Chihchen Chen, Nicholas L. Stucky, and Albert Folch*

Department of Bioengineering, University of Washington, Seattle WA 98195, USA

We present a batch-fabricated, biocompatible and optically transparent lab-on-a-chip device that incorporates a planar array of nanoholes that can potentially be used for electrical or pharmacological interrogation of large numbers of cells as well as for precise biochemical delivery to cells. The nanoholes are defined in a silicon nitride layer using electron beam lithography and chemical etching techniques. Each nanohole in the array is microfluidically accessible and individually addressable from both sides via a PDMS microchannel network, allowing for rapid perfusion and exchange of fluids. A thin PDMS layer between the silicon nitride and the PDMS microchannels electrically isolates each nanohole. The electrical properties of our nanohole devices are within the typical range for traditional glass patch-clamp micropipettes of similar diameters and appear suitable for low-current measurements of ion diffusion through the nanoholes. Various types of cells cultured in these devices proliferated normally, showing the biocompatibility of our devices. We have also demonstrated the efficacy of our nanohole device for studies of cell chemotaxis using interleukin-8 directed migration of neutrophils as our model system.

Keywords: Nanohole, Nanoaperture, Electron Beam Lithography, Soft Lithography, BioMEMS, Microfluidics, Patch-Clamp, Electrophysiology, Focal Delivery, Neutrophil Chemotaxis

RESEARCH ARTICLE

1. INTRODUCTION

Micron- and submicron-size holes or apertures ("nanoholes") are used in many cell and molecular biology applications. They come in two different configurations: (1) the tip of a micropipette, or (2) a pore communicating the two sides of a thin membrane. Micropipettes are fabricated by heating a glass capillary in its middle section while pulling its ends to produce a nanohole at the end of a tapered tip where the capillary splits. Micropipettes are inexpensive, are readily available in many biomedical laboratories, and have been widely used for decades for single-cell injection (reviewed in Ref. [1]), patch-clamp electrophysiology (reviewed in Ref. [2]), iontophoretic stimulation[3,4] (reviewed in Ref. [5]), and "puffing" (pressure ejection) delivery of gradients of signaling factors (reviewed in Ref. [5]). In addition, micropipettes can be used for mechanical manipulation of single cells, e.g., to bring a given cell into contact with other cells for secretion studies[6] or to sever a portion of the cell membrane for cellular transport studies,[7] among other applications. Unfortunately, micropipette techniques generally require substantial operator expertise and suffer from low throughput and high failure rates. Expensive micromanipulators are also required to precisely position the micropipette, and mechanical vibration and drift are common sources of failure in electrophysiological applications.[8] Additionally, due to the fragility and bulky geometry of micropipettes, they are difficult to incorporate into arrays.

Planar nanoholes promise to overcome the limitations of micropipettes, however they also face fabrication challenges if they are to be suitable for routine use. In contrast to the heat-and-pull simplicity of producing micropipettes, planar nanoholes are fabricated using micro- and nanofabrication techniques[9,10] such as ion track etching,[11,12] ion-beam sculpting,[13] electron-beam lithography (EBL),[14] conventional silicon-based techniques[15–17] or elastomeric micromolding of a point-contact in poly(dimethylsiloxane) (PDMS).[18] Planar nanoholes have been used for cellular immunoisolation,[15] biomolecular separation,[15] chip-based patch-clamping,[12,17–20] lipid bilayer-based single ion channel studies,[16] and show potential for use in single-molecule DNA sequencing.[13] However, the present planar

*Author to whom correspondence should be addressed.

 1550-7033/2005/1/001/007/$17.00+.25 doi:10.1166/jbn.2005.023

nanohole fabrication approaches have several limitations. Ion-track etching and ion-beam sculpting both require prohibitively expensive equipment not available to most researchers. PDMS micromolding of a point-contact[18] (i.e., replica-molding of two bodies that are pressed in contact at a few points) is limited by the difficulty to control the contact point area as a function of applied pressure (resulting in holes not significantly smaller than a micrometer and with irregular, hardly reproducible shapes).

In this study, we explore an alternative approach for planar nanohole fabrication that is easily fabricated and meets basic criteria for several assay techniques. We present a robust, optically transparent device that incorporates a planar array of nanoholes that can potentially be used for electrical or pharmacological interrogation as well as biochemical stimulation of large numbers of cells in parallel. The nanoholes are defined using EBL, which is commonly available in most research universities and is capable of generating features with dimensions on the order of tens of nanometers. Additionally, the EBL patterns are software-generated and not in physical form like in other lithographic techniques, allowing for easy and inexpensive scaling and design iterations. Most of the fabrication steps are appropriate for large batches, which reduce fabrication time and lower production costs. Additionally, our device is biocompatible, in the sense that cells can be cultured on it for several days. Each nanohole in the array is microfluidically accessible and individually addressable from one or both sides (depending on the assay requirements), allowing for rapid perfusion, delivery, and exchange of fluids. Each nanohole is fluidically and electrically isolated from all the others in the array as well as from the rest of the substrate—essentially behaving like the nanohole of a micropipette—, which makes them suitable for low-current measurements of ion diffusion through the nanoholes.

We also show the efficacy of our nanohole device for studying cell chemotaxis—the ability of cells to sense gradients of extracellular molecules and to migrate towards attractants and away from repellents[21]—using interleukin-8 (IL-8) directed migration of neutrophils as a model system. Neutrophils, formally known as neutrophilic polymorphonuclear leukocytes, are the most abundant white cells in the blood.[22] They play a crucial role in the body's response to injuries and are the primary defense against infections.[23] By correctly interpreting and following the gradients of specific chemotactic factors released from the affected areas, such as interleukin-1 (IL-1) and IL-8, these cells migrate to and accumulate at the sites of inflammation and kill the invading organisms.[24,25] Neutrophil chemotaxis has been qualitatively studied *in vitro* since 1917.[26] Several techniques and tools have been developed to create gradients of chemotactic factors and study chemotaxis, such as Boyden chamber,[27] Zigmond chamber,[28] Dunn chamber,[29] and microfabricated devices.[30] However, none of them are capable of generating stable and well-defined gradients of chemotactic factors diffusing from a point source (as found *in vivo*) in a straightforward and high-throughput manner. To demonstrate the efficacy of our device in studying this complex system, we used our device to establish concentration gradients of IL-8 diffusing out of the nanoholes, acting as point sources, and observed the migration of human neutrophils towards the nanoholes. In addition to neutrophil migration, our nanohole device promises to be equally useful for other similar cell migration applications.

2. MATERIALS AND METHODS

2.1. Silicon Device Fabrication

Using a low pressure chemical vapor deposition (LPCVD) system, we first deposited a 300 nm layer of silicon-rich (i.e., low-stress) silicon nitride (LSN) onto a 3 in.-diameter, 400 μm-thick Si$\langle 100 \rangle$ wafer (Silicon Sense, Inc., NH) (Fig. 1A). In an electron-beam evaporation system, a 10 nm-thick layer of chromium (to facilitate adhesion of gold) followed by a 100 nm-thick layer of gold was deposited on the front (polished) side of the wafer (Fig. 1B). Gold alignment marks as reference points for subsequent lithography processes were created by standard photolithographic techniques using AZ1512 photoresist (Clariant Corporation, AZ) and a 3600 dpi transparency photomask (Publication Services, University of Washington, WA) followed by Au and Cr wet etching (Fig. 1C). A 750 nm-thick layer of poly(methylmethacrylate) (PMMA) EBL resist (NANO 950 PMMA A 6; MicroChem Corp., MA) was spin-coated onto the front side of the wafer. Using a scanning electron microscope (SEM) (Sirion; FEI Company, OR) interfaced to an EBL system (Nabity Lithography Systems, MT) to scan the electron beam, an array of (sub)micron-diameter dots was exposed in the PMMA film in registry with the alignment marks. The wafer was then developed in PMMA Developer (MicroChem Corp., MA), which selectively dissolves the exposed sections of the PMMA film, leaving cylindrical holes in the PMMA layer. This process can generate features with linewidths ranging from tens of nanometers to tens of micrometers. Using the PMMA layer to mask a reactive ion etch (RIE) with SF_6 as the etching gas, the array of holes was transferred into the LSN layer. The residual PMMA was then removed in an acetone bath (Fig. 1D). Next, square "windows" with 760 μm sides were formed in the LSN layer on the backside of the wafer by standard photolithographic techniques (using AZ1512 photoresist and a second film photomask, again in registry with the alignment marks on the front side) followed by RIE with SF_6 as the etching gas (Fig. 1E). An aligner/exposer system with backside infrared illumination (AB-M, Inc., CA) was used to visualize the frontside gold alignment marks through the wafer;

RESEARCH ARTICLE

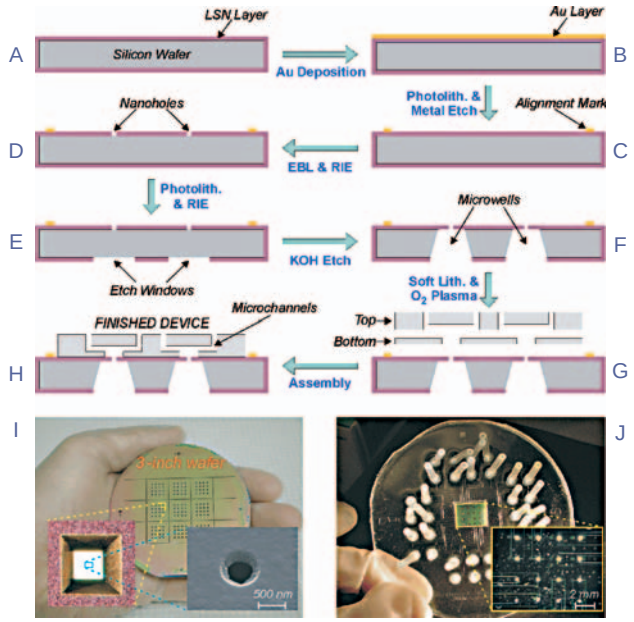

Fig. 1. (A–H) Fabrication of the nanohole device: First, a thin layer of LSN is deposited on the whole wafer (A) followed by a layer of gold on the front (polished) side of the wafer (B). Using photolithography and gold etching, gold alignment marks are created (C). Next, nanoholes, which are in registration with the alignment marks, are etched in the LSN layer using e-beam lithography followed by RIE (D). Etch windows, which are in registration with the alignment marks, are patterned in the LSN layer on the back side of the wafer via photolithography followed by RIE (E). The wafer is then immersed in KOH bath, which anisotropically etches inverted-pyramid pits (microwells) until the pits reach the bottom of the front LSN layer and creates an array of suspended LSN membranes with a nanohole at the center of each membrane (F). To address each of the nanoholes microfluidically, a microchannel network made of PDMS is fabricated using soft lithographic methods (G). Last, the complete PDMS microchannel network is bonded onto the front side of the wafer in registration with the suspended LSN membranes (H). (I) Backside of a wafer (after step F) with nine identical chips (in a 3×3 array), each with a 4×4 array of microwells; the inset (yellow) shows a magnified view of a microwell and the inset (cyan) shows SEM image of a suspended LSN membrane with a 500 nm diameter hole at its center. (J) Top view of a finished device; the inset shows a PDMS microchannel network underneath the silicon chip.

the only purpose of the gold features is thus to serve as a reference for proper alignment of the backside LSN windows and the frontside LSN nanoholes. The wafers were then immersed in a KOH bath (5 M, 80 °C), which anisotropically etched inverted-pyramid pits[9] in the backside (which we term "microwells"), until the pits reached the bottom of the front LSN layer. This process created an array of suspended LSN membranes with a nanohole at the center of each membrane (Fig. 1F).

2.2. Fabrication of PDMS Microchannel Network

To address each of the nanoholes microfluidically, a microchannel network made of PDMS—a transparent biocompatible elastomer (Sylgard 184; Dow Corning, MI)—was fabricated using soft lithographic methods[31] independently of the wafer containing LSN membranes. First, using SU-8 negative photoresist (MicroChem Corp., MA) and high-resolution acetate film photomasks (Publication Services, University of Washington), two master mold patterns were formed on silicon wafers and replicated in PDMS using standard soft lithography processes.[31] The first (bottom) PDMS replica was designed to incorporate square openings (microfluidic windows) spatially matching (but with sides at least 25% shorter than) the suspended LSN membranes, whereas the second (top) replica formed the microchannels, which connected the microfluidic windows to the inlets and outlets (Fig. 1G). After the surfaces of the two PDMS layers have been chemically activated using oxygen plasma exposure in order to get a robust, permanent bond,[32] they were aligned and sealed together.

2.3. Assembly of PDMS Microchannel Network to Silicon Device

The complete PDMS microchannel network was assembled onto the front side of the wafer in registry with the suspended LSN membranes. The LSN and the PDMS surfaces were chemically activated using an oxygen plasma exposure prior to assembly.[32] A good alignment between the wafer and the PDMS microchannel network was achieved by suspending the PDMS on top of the wafer using four pea-sized clay balls placed around the edges, aligning both parts under a dissection microscope, and gently pressing the PDMS onto the wafer (starting from the middle). Once the seal formed in the center, the flattened clay balls were removed to allow the rest of the surface to come in contact and bond (Fig. 1H). The design can be easily altered to permit access to the microfluidic inlets from either the front side or the backside of the wafer as required by a specific experimental setup.

2.4. Electrical Characterization of the Nanohole Device

Standard electrolytic patch-clamping solution (Ringer's solution) was dispensed into a microwell and injected into its corresponding microchannel, at which point both sides of the LSN membrane contacted the solution (Fig. 2A). Two Ag/AgCl electrodes were immersed into the solutions, one in the microwell and the other at the inlet of the corresponding microchannel. A patch-clamp amplifier (Multiclamp 700A; Axon Instruments Inc., CA) was used to apply a square-wave voltage signal across the electrodes and record the resultant current trace. Resistance was obtained using Ohm's law by dividing the steady state current by the voltage change. The capacitance was measured by two different methods: (1) numerically integrating the transient current following the voltage change; (2) using the built-in patch-clamp amplifier capacitance compensation feature (pCLAMP 8.0; Axon Instruments Inc., CA). The capacitance of the amplifier and associated wiring was

RESEARCH ARTICLE

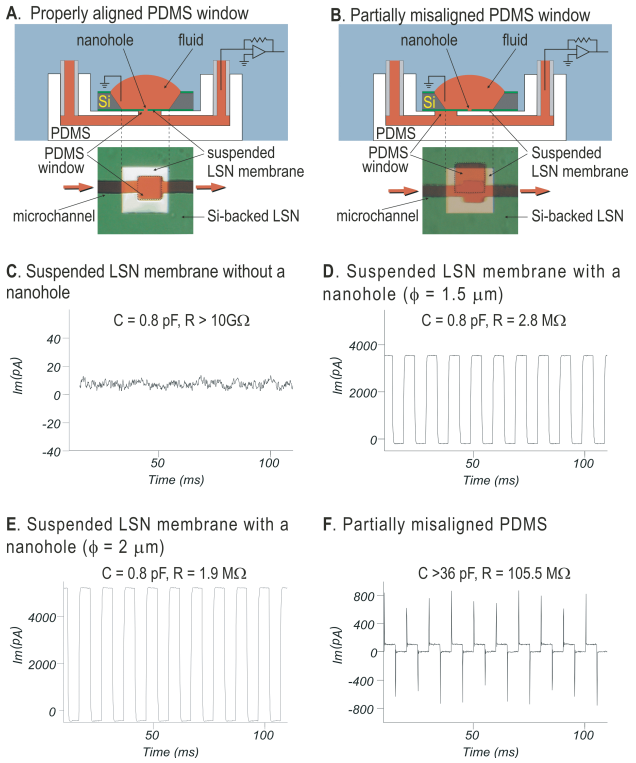

Fig. 2. (A–B) Cross-sectional schematics of the nanohole devices (top) and top-view micrograph (bottom). The microchannel was filled with red dye, the unsuspended LSN appears green, and the suspended LSN appears white (transparent). Ag/AgCl wires for electrical characterization were inserted at the locations as shown. A illustrates a properly aligned PDMS window, whereas in B the PDMS window is partially misaligned, hence exposing a section of the silicon-backed LSN layer. (C-E) Resistance and capacitance measurements using properly-aligned devices (e.g., as shown in A) featuring 0 nm- (C), 1500 nm- (D) and 2000 nm-diam. (E) nanoholes, respectively. Shown are the current responses to a 10 mV amplitude square wave voltage command; capacitive transients have been subtracted. (F) Resistance and capacitance of device shown in B with a misaligned PDMS window which blocks the nanohole; here, capacitive transients could not be fully subtracted (see text for details).

measured separately and subtracted from the total capacitance to yield the stray capacitance of the device alone.

2.5. Biocompatibility of the Nanohole Device

The cells were seeded on the LSN membranes of the nanohole devices. All cell cultures were incubated in a water-jacketed CO_2 incubator with HEPA filtration (Series II; Forma Scientific, OH) at 37 °C under a humidified atmosphere of 5% CO_2 and 95% air for several days. Mouse fibroblasts (NIH/3T3), Chinese hamster ovary cells (CHO-K1), human embryonic kidney cells (HEK293), and mouse myoblasts (C2C12) were purchased from American Type Culture Collection (ATCC, VA). NIH/3T3 cells were cultured in Dulbecco's Modified Eagle's Medium (DMEM; GIBCO/Invitrogen Corporation, CA) supplemented with 10% heat-inactivated newborn calf serum (GIBCO/Invitrogen) and inoculated with 1% penicillin-streptomycin solution (Pen-Strep; GIBCO/Invitrogen). CHO-K1 cells were cultured in Ham's F12K medium with 2 mM L-glutamine adjusted to contain 1.5 g/L sodium bicarbonate (ATCC), supplemented with 10% fetal bovine serum (GIBCO/Invitrogen), and inoculated with 1% Pen-Strep. HEK293 cells were cultured in Eagle's minimal essential medium with Earle's Balanced Salt Solution and 2 mM L-glutamine that is modified by ATCC to contain 1.0 mM sodium pyruvate, 0.1 mM nonessential amino acids, and 1.5 g/L sodium bicarbonate (ATCC), supplemented with 10% heat-inactivated horse serum (ATCC), and inoculated with 1% Pen-Strep. C2C12 cells were cultured in DMEM (GIBCO/Invitrogen) supplemented with 20% fetal bovine serum and inoculated with 1% Pen-Strep. All cell cultures were grown to 90% confluence.

2.6. Time-Lapse Microscopy of Neutrophil Chemotaxis

Neutrophils isolated from the blood of human subjects were suspended in Hanks' Balanced Salt Solution (HBSS) (GIBCO/Invitrogen) with 0.1% Bovine Serum Albumin (BSA) (Sigma, MO) at a concentration of 10^6 cells/ml. The cells were seeded on the flat (membrane) side of the device and allowed to settle to the LSN surface. The device was then turned upside down and sealed to the bottom of a 35 mm petri dish. The microwell side of the device (now facing upward) was filled with IL-8 (Sigma) solution (1 μg/ml in HBSS) and covered with a coverslip to minimize evaporation (Fig. 3A). Time-lapse microscope images of the neutrophils migrating towards the nanoholes, which were serving as point sources of IL-8, were taken using an inverted microscope (Eclipse TE2000-U; Nikon, Japan) in phase contrast mode at two-minute intervals.

3. RESULTS AND DISCUSSION

3.1. Fabrication of the Nanohole Device

Figures 1A through 1H illustrate the fabrication flow of the nanohole device. Using standard fabrication procedures, we were able to create nanoholes as small as 50 nm in diameter in suspended LSN membranes. (See the Methods section for a step-by-step explanation of the flow process.) Figure 1I is an image of the backside of a finished wafer with nine identical devices, with the inset (yellow) showing a magnified view of a microwell and the inset (cyan) showing an SEM image of a finished 220 μm-wide, 300 nm-thick suspended LSN membrane with a 500 nm diameter hole at the center. Figure 1J is the top view of a finished device, with the inset showing a PDMS microchannel network underneath the silicon chip.

3.2. Electrical Properties of the Nanohole Device

Measuring the passage of ions through nanoholes is paramount in electrophysiological recordings of electrically-active cells,[33] in the study of bilayer-embedded synthetic

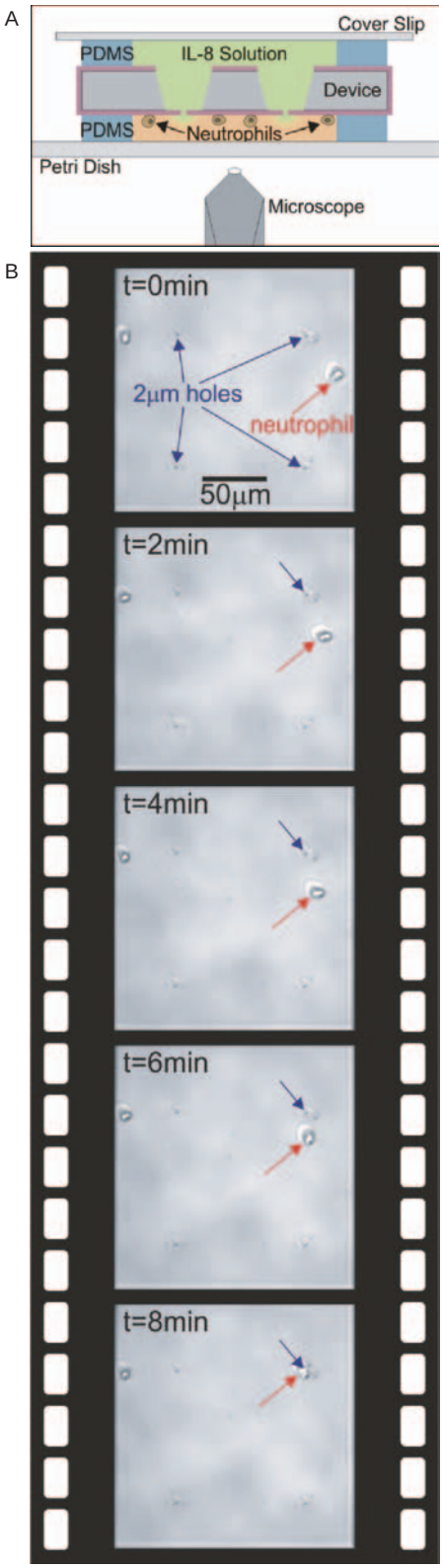

Fig. 3. **(A)** Schematic cross-sectional illustration of the experimental setup for studying neutrophil chemotaxis. **(B)** 8-minute time-lapse sequence of phase-contrast micrographs showing the migration of a single human neutrophil towards the nearest of the four 2 μm-diam. holes, which is acting as a point source of IL-8.

ion channels,[16,34] and in probing DNA structure as the molecule passes through the hole,[13] to cite a few examples. To evaluate the suitability of the device for measurements of ionic currents through the nanoholes, we measured the resistance and capacitance of a fluidic circuit that connected a microwell through the nanohole to its corresponding fluidic inlet; Figure 2A shows the schematic cross-section and top-view micrograph of the device when the LSN membrane was properly aligned to the PDMS window (the microchannel was filled with red dye for visualization and the silicon-backed LSN appears green). Compared to the topology of a traditional electrophysiology micropipette, the microchannel side of the suspended LSN membrane in our device is analogous to the inside of the micropipette and the microwell side of the suspended LSN membrane is analogous to the outside of the micropipette. The measured capacitance of our microdevice is similar to that of a micropipette within 10%. The capacitance-compensated current responses to the square wave voltage command are shown in Figures 2C–E for nanohole diameters of 0 (no hole), 1.5 μm, and 2 μm; the measured resistances were >10 GΩ (too high to measure with our electronics setup), 2.8 MΩ, and 1.9 MΩ, respectively, whereas the measured capacitances were on the order of 0.8 pF in all cases. Figure 2C shows that the suspended LSN membrane without a nanohole is a very effective insulator (R > 10 GΩ), as no measurable current flows through the device without a nanohole. To test the effect of PDMS insulation, the microfluidic window was (purposefully) partially misaligned as shown in Figure 2B. In this case, the nanohole was completely blocked by PDMS, and part of the Si-backed part of the LSN layer was exposed. This results in large capacitive transients (>36 pF) which could not be fully compensated for by the amplifier as shown in Figure 2F. Additionally, the two sides of the LSN membrane are not fully electrically isolated when (due to the partial misalignment of the PDMS window) the Si-backed LSN is exposed to fluid, as shown by the very low resistance in Figure 2F ($\sim$100 MΩ, nanohole blocked and Si-backed LSN exposed to electrolytic solution) compared to Figure 2C (R > 10 GΩ, no nanohole but no Si-backed LSN is exposed to electrolytic solution). Thus, we conclude that the Si-backed part of the LSN layer is not a good ion insulator (possibly caused by the fact that LSN is a thin, silicon-rich material in intimate contact with silicon, a very good charge donor), whereas freestanding LSN is an excellent ion insulator. Hence the PDMS microfluidic windows in our device were designed to be smaller than the suspended LSN membranes so they effectively isolated the rest of the fluidic network from the underlying Si-backed LSN surface when properly aligned. Taken together, these results indicate that the electrical isolation of the fluidic path by its all-PDMS walls on one side of the device is crucial to the performance of the device.

Low-current recordings of ion diffusion through nanoholes also require a low resistance between the two Ag/AgCl electrodes (when a nanohole is present) and low stray capacitance to ground. Figures 2D and 2E show the current traces, resistance and capacitance values for devices with 1.5 and 2.0 μm diameter nanoholes, respectively. As expected, the resistance decreases with increasing nanohole diameter. The resistances (1.9–2.8 MΩ) for the 1.5 and 2.0 μm-diam. nanoholes in Figures 2D and 2E are within the typical range for traditional glass patch-clamp micropipettes of similar nanohole diameter (1–10 MΩ).[35,36] The stray capacitances ($\sim$0.8 pF) are slightly higher than those of traditional micropipettes (<0.25 pF) but well within the range of the patch-clamp amplifier's capacitance compensation capabilities (tens of pF). The slightly larger capacitance of our device compared to traditional micropipettes can probably be attributed to the larger surface area of the device fluidics, which can in principle be reduced in future designs by minimizing the fluidic path lengths/widths and/or by optimizing the placement of the Ag/AgCl electrodes. Since low device resistance and capacitance are essential for decreasing the background noise levels in patch clamp recording, our nanohole device may be suitable for low-current (such as patch-clamp) measurements. For particular applications, other (to be tested) requirements may be needed; for example, it remains to be determined whether live cells (or which cells) can form high resistance ("gigaohm") seals with cells, another important requirement for patch-clamp applications.[35]

3.3. Biocompatibility of Nanohole Device

In this device cells may contact surfaces of both PDMS and LSN. PDMS has been increasingly used in biological applications and is shown to be compatible with mammalian cell lines.[37] Additionally, silicon nitride has been targeted for development of implants and has been shown to support proliferation of human cell lines.[38] To assess the biocompatibility of the finished device—more specifically, the ability of the LSN surface to support cell attachment and growth after microfabrication processing–we cultured NIH/3T3, CHO-K1, HEK293, and C2C12 cells (a skeletal muscle cell line) for several days inside microwells and/or on the flat (membrane) side of the device. All cultures appeared morphologically normal and viable, and proliferated comparably to the controls grown in tissue culture dishes.

3.4. Neutrophil Chemotaxis

Last, we evaluated our nanohole device for controlled delivery of biochemical factors to cells as a method for modulating the fluidic microenvironment of cells in culture. As an example, we tested its efficacy for studying cell chemotaxis. As our model system, we chose the directed migration of neutrophils towards the chemoattractant IL-8. Figure 3A illustrates our experimental setup in cross-section view. The nanoholes served as the only conduits for IL-8 to diffuse into the lower cell culture chamber. Phase contrast micrographs were used to document neutrophil migration towards the IL-8 releasing holes. The time-lapse sequence of five images in Figure 3B, which were taken at 2-minute intervals, shows the movement of a single human neutrophil towards the nearest of four transmembrane holes (2 μm diameter), which is acting as a point source of IL-8. More work is underway to determine the distribution of migration rates as single neutrophils migrate towards the evolving point source, a good *in-vivo* analog of the injury repair process whereby neutrophils are recruited to the wound sites by IL-8-secreting cells.

4. CONCLUSIONS

In summary, we have presented a biocompatible device that incorporates arrays of microfluidically-addressable nanoholes on transparent membranes that is easy to fabricate and to scale up. The device has electrical properties suitable for electrophysiological studies that require the measurement of ionic currents through nanoholes. Our device can potentially be used for a range of applications in cell biology and high-throughput screening that require simultaneous electrical, optical and/or pharmacological interrogation of a large number of cells. Compared to other planar nanohole approaches,[12,17–19] our device is inexpensive, scalable, simple to use, and straightforwardly fabricated as a reliable microarray for highly parallel measurements. Additionally, the small volume and addressability of the microwells and channels allows for electrical interrogation to be combined with (or replaced by) focal delivery of biomolecules or pharmacological agents. By forming concentration gradients of chemotactic factors using the nanoholes as point sources, we have also demonstrated the efficacy of our nanohole device for future studies of cell chemotaxis. Because of the optical transparency of thin LSN membranes, various types of microscopy, fluorescence and photometric techniques can also be used. In sum, the device presented here is a versatile, inexpensive tool that meets basic criteria for a number of powerful biological assay techniques.

Acknowledgments: We are grateful to Prof. Charles W. Frevert at the University of Washington, Veterans Administration Medical Center, for providing human neutrophils. We also acknowledge the help and support provided by the staff members of the Washington Technology Center and the Nanotechnology User Facility at the University of Washington. This work was partially funded by the Whitaker Foundation (grant # RG-00-0356), NASA (grant # NAG9-1343), NIH (grant # RR16302), and the UW Center for Nanotechnology (fellowship to T. F. K.).

References and Notes

1. K. T. Brown and D. G. Flaming, Advanced micropipette techniques for cell physiology. Ibro handbook series, Wiley, Chichester [West Sussex], New York, x, **(1986)**, Vol. 9, p. 296.
2. A. A. Boulton, G. A. Baker, and W. Walz, eds. Patch-clamp applications and protocols. *Neuromethods*, Humana Pr. **(1995)**, Vol. 26.
3. W. L. Nastuk, The electrical activity of the muscle cell membrane at the neuromuscular junction. *J. Cell. Comp. Physiol.* 42, 249 **(1953)**.
4. J. del Castillo and B. Katz, On the localization of acetylcholine receptors. *J. Physiol.* 128, 157 **(1955)**.
5. T. W. Stone, Microiontophoresis and pressure ejection. 1st ed., John Wiley & Sons, Incorporated, **(1985)**, Vol. 8, p. 214.
6. I. Chow and M. M. Poo, Release of acetylcholine from embryonic neurons upon contact with muscle-cell. *J. Neurosci.* 5, 1076 **(1985)**.
7. D. Y. Gao, J. J. McGrath, J. Tao, C. T. Benson, E. S. Critser, and J. K. Critser, Membrane transport properties of mammalian oocytes: A micropipette perfusion technique. *J. Reprod. Fertil.* 102, 385 **(1994)**.
8. F. Sachs, A low drift micropipette holder. *Pflugers Arch.* 429, 434 **(1995)**.
9. M. J. Madou, Fundamentals of microfabrication: The science of miniaturization. 2nd ed., CRC Press, Boca Raton, 723 **(2002)**.
10. H. C. Hoch, L. Jelinski, and H. G. Craighead, Nanofabrication and biosystems: Integrating materials science, engineering, and biology. Cambridge University Press, Cambridge; New York, NY, xviii, 423 **(1996)**.
11. N. Fertig, C. Meyer, R. H. Blick, C. Trautmann, and J. C. Behrends, Microstructured glass chip for ion-channel electrophysiology. *Phys. Rev. E* 6404, art. no. 040901 **(2001)**.
12. N. Fertig, R. H. Blick, and J. C. Behrends, Whole cell patch clamp recording performed on a planar glass chip. *Biophys. J.* 82, 3056 **(2002)**.
13. J. Li, D. Stein, C. McMullan, D. Branton, M. J. Aziz, and J. A. Golovchenko, Ion-beam sculpting at nanometre length scales. *Nature* 412, 166 **(2001)**.
14. N. Fertig, A. Tilke, R. H. Blick, J. P. Kotthaus, J. C. Behrends, and G. ten Bruggencate, Stable integration of isolated cell membrane patches in a nanomachined aperture. *Appl. Phys. Lett.* 77, 1218 **(2000)**.
15. T. A. Desai, D. J. Hansford, and M. Ferrari, Micromachined interfaces: New approaches in cell immunoisolation and biomolecular separation. *Biomol. Eng.* 17, 23 **(2000)**.
16. C. Schmidt, M. Mayer, and H. Vogel, A chip-based biosensor for the functional analysis of single ion channels. *Angew. Chem.-Int. Edit.* 39, 3137 **(2000)**.
17. T. Lehnert, M. A. M. Gijs, R. Netzer, and U. Bischoff, Realization of hollow sio2 micronozzles for electrical measurements on living cells. *Appl. Phys. Lett.* 81, 5063 **(2002)**.
18. K. G. Klemic, J. F. Klemic, M. A. Reed, and F. J. Sigworth, Micromolded pdms planar electrode allows patch clamp electrical recordings from cells. *Biosens. Bioelectron.* 17, 597 **(2002)**.
19. K. G. Klemic, W. T. Baker, J. F. Klemic, M. A. Reed, and F. J. Sigworth, Patch clamping with a planar electrode array. *Biophys. J.* 80, 1412 **(2001)**.
20. J. Xu, X. B. Wang, B. Ensign, M. Li, L. Wu, A. Guia, and J. Q. Xu, Ion-channel assay technologies: Quo vadis? *Drug Discov. Today* 6, 1278 **(2001)**.
21. M. Iijima, Y. E. Huang, and P. Devreotes, Temporal and spatial regulation of chemotaxis. *Dev. Cell* 3, 469 **(2002)**.
22. S. W. Edwards, Biochemistry and physiology of the neutrophil. Cambridge University Press, Cambridge England; New York, xviii, 299 **(1994)**.
23. F. Mollinedo, N. Borregaard, and L. A. Boxer, Novel trends in neutrophil structure, function and development. *Immunol. Today* 20, 535 **(1999)**.
24. M. Baggiolini, Chemokines and leukocyte traffic. *Nature* 392, 565 **(1998)**.
25. F. Lin, C. M. Nguyen, S. J. Wang, W. Saadi, S. P. Gross, and N. L. Jeon, Effective neutrophil chemotaxis is strongly influenced by mean il-8 concentration. *Biochem. Biophys. Res. Commun.* 319, 576 **(2004)**.
26. C. W. Frevert, V. A. Wong, R. B. Goodman, R. Goodwin, and T. R. Martin, Rapid fluorescence-based measurement of neutrophil migration in vitro. *J. Immunol. Methods* 213, 41 **(1998)**.
27. S. Boyden, The chemotactic effect of mixtures of antibody and antigen on polymorphonuclear leucocytes. *J. Exp. Med.* 115, 453 **(1962)**.
28. S. H. Zigmond, Ability of polymorphonuclear leukocytes to orient in gradients of chemotactic factors. *J. Cell. Biol.* 75, 606 **(1977)**.
29. D. Zicha, G. A. Dunn, and A. F. Brown, A new direct-viewing chemotaxis chamber. *J. Cell. Sci.* 99, 769 **(1991)**.
30. N. L. Jeon, H. Baskaran, S. K. W. Dertinger, G. M. Whitesides, L. Van de Water, and M. Toner, Neutrophil chemotaxis in linear and complex gradients of interleukin-8 formed in a microfabricated device. *Nat. Biotechnol.* 20, 826 **(2002)**.
31. Y. N. Xia and G. M. Whitesides, Soft lithography review. *Annu. Rev. Matr. Sci.* 28, 153 **(1998)**.
32. D. C. Duffy, J. C. McDonald, O. J. A. Schueller, and G. M. Whitesides, Rapid prototyping of microfluidic systems in poly (dimethylsiloxane). *Anal. Chem.* 70, 4974 **(1998)**.
33. E. Neher, Ion channels for communication between and within cells. *Science* 256, 498 **(1992)**.
34. B. E. Ehrlich, Planar lipid bilayers on patch pipettes: Bilayer formation and ion channel incorporation. *Methods Enzymol.* 207, 463 **(1992)**.
35. O. P. Hamill, A. Marty, E. Neher, B. Sakmann, and F. Sigworth, Improved patch-clamp techniques for high-resolution current from cells and cell-free membrane patches. *Pflugers Arch.* 391, 85 **(1981)**.
36. B. Sakmann and E. Neher, Single-channel recording. 2nd ed., Plenum Press, New York, xxii, 700 **(1995)**.
37. J. N. Lee, X. Jiang, D. Ryan, and G. M. Whitesides, Compatibility of mammalian cells on surfaces of poly(dimethylsiloxane). *Langmuir* 20, 11684 **(2004)**.
38. R. Kue, A. Sohrabi, D. Nagle, C. Frondoza, and D. Hungerford, Enhanced proliferation and osteocalcin production by human osteoblast-like mg63 cells on silicon nitride ceramic discs. *Biomaterials* 20, 1195 **(1999)**.

Received: XX Xxxxx XXXX. Accepted: XX Xxxxxxx XXXX.

RESEARCH ARTICLE